ChemPubSoc Europe

DOI: 10.1002/chem.201305072

CHEMISTRY
A European Journal
Full Paper

Magnetic Nanoparticles

General Protocol for the Synthesis of Functionalized Magnetic Nanoparticles for Magnetic Resonance Imaging from Protected Metal–Organic Precursors

He Hu, Chongkun Zhang, Lu An, Yanrong Yu, Hong Yang, Jin Sun, Huixia Wu, and Shiping Yang*[a]

Abstract: The development of magnetic nanoparticles (MNPs) with functional groups has been intensively pursued in recent years. Herein, a simple, versatile, and cost-effective strategy to synthesize water-soluble and amino-functionalized MNPs, based on the thermal decomposition of phthalimide-protected metal–organic precursors followed by deprotection, was developed. The resulting amino-functionalized Fe_3O_4, $MnFe_2O_4$, and Mn_3O_4 MNPs with particle sizes of about 14.3, 7.5, and 6.6 nm, respectively, had narrow size distributions and good dispersibility in water. These MNPs also exhibited high magnetism and relaxivities of $r_2 = 107.25\ mM^{-1}s^{-1}$ for Fe_3O_4, $r_2 = 245.75\ mM^{-1}s^{-1}$ for $MnFe_2O_4$, and $r_1 = 2.74\ mM^{-1}s^{-1}$ for Mn_3O_4. The amino-functionalized MNPs were further conjugated with a fluorescent dye (rhodamine B) and a targeting ligand (folic acid: FA) and used as multifunctional probes. Magnetic resonance imaging and flow-cytometric studies showed that these probes could specifically target cancer cells overexpressing FA receptors. This new protocol opens a new way for the synthesis and design of water-soluble and amino-functionalized MNPs by an easy and versatile route.

Introduction

Magnetic nanoparticles (MNPs) have shown great promise for diagnostic and therapeutic applications.[1] Since the particle sizes of MNPs are smaller than the critical size, they are in a superparamagnetic state at room temperature, and this results in unique opportunities for magnetic separation, targeted drug delivery, hyperthermic therapy, and contrast agents for magnetic resonance imaging (MRI).[1b,c,2] MRI is noninvasive, one of the most powerful diagnostic techniques for living organisms, and is based on the response of protons of tissues to an applied external magnetic field.[3] With the help of MNPs as contrast agents, it is possible to provide greater contrast and obtain information-rich images for disease diagnosis and therapy.[1a,4] However, MNPs utilized as contrast agents for MRI must have good dispersibility, stability, biocompatibility, water solubility, and functional groups on their surfaces to conjugate with biomolecules.[1a,b,5]

Until now, different techniques have been developed for the preparation of MNPs, such as coprecipitation, microemulsification, and solvothermal and thermal decomposition.[1b,c,6] Some water-soluble MNPs, especially iron oxide MNPs, could be directly prepared by coprecipitation in high yields by using functional small molecules or polymers as stabilizers.[7] Nevertheless, control of the particle size, dispersion, and magnetic properties through this route is still very limited.[8] Solvothermal synthesis is another effective method for the preparation of water-soluble and well-crystallized MNPs.[9] Unfortunately, the large particle size (>100 nm) and lack of functional groups on the surface of the MNPs prevented their further biological applications.[1b,c,2] Recently, an alternative method has been developed to prepare high-quality MNPs by the thermal decomposition of different types of organometallic compounds or metal–surfactant complexes, such as iron carbonyls ($[Fe(CO)_5]$),[10] iron oleates,[11] and metal triacetylacetonates ($M(acac)_3$; M = Fe, Co, Mn),[12] in a high-boiling-point organic solvent with oleic acid (OA) and/or oleylamine (OAm) as surfactants. These as-prepared NPs have good shape control, high crystallinity, and high monodispersibility.[13] For example, Weissleder et al. prepared core–shell MNPs by the decomposition of $Fe(CO)_5$.[10] Hyeon and co-workers reported large-scale syntheses of monodisperse MNPs by the decomposition of an iron oleate complex, and their results demonstrated that a metal–surfactant complex is an effective growth source for the synthesis of monodisperse nanocrystals.[11] Sun et al. synthesized MNPs using $M(acac)_3$ as starting materials.[12] However, all these MNPs prepared by thermal decomposition are only soluble in nonpolar organic solvents without surface modifications that greatly inhibit their bioapplications.[1a,5]

[a] Dr. H. Hu, C. Zhang, L. An, Y. Yu, Dr. H. Yang, J. Sun, Dr. H. Wu, Dr. S. Yang
The Key Laboratory of the Resource Chemistry of Ministry of Education
and the Shanghai Key Laboratory of the Rare Earth Functional Materials
Department of Chemistry, Shanghai Normal University
No. 100 Guilin Road, Shanghai, 200234 (P. R. China)
Fax: (+86) 21-64322511
E-mail: shipingy@shnu.edu.cn

Supporting information for this article is available on the WWW under http://dx.doi.org/10.1002/chem.201305072.

More recently, modified one-step thermal-decomposition protocols to prepare water-soluble MNPs have been developed. For instance, Gao et al. prepared water-soluble MNPs by thermal decomposition of $Fe(acac)_3$ in 2-pyrrolidone, which not only served as the medium for the high-temperature reaction, but also acted as a surface stabilizer making the MNPs water-soluble.[14] Recently, we developed a facile route for the synthesis of water-soluble superparamagnetic $MnFe_2O_4$ NPs by the decomposition of $M(acac)_3$ in tetraethylene glycol (TEG) solvent.[15] Here, the TEG acts as a stabilizer to control the particle growth and prevent the aggregation of particles in the high-temperature reaction medium. However, these endeavors still have not solved the problem of functionalizing the NPs. Therefore, a facile and general approach for directly synthesizing water-soluble MNPs with multiple functional groups is necessary.

The greatest problem when preparing functional NPs is that the active groups (e.g., NH_2, COOH, SH) readily react with other compounds during NP formation. On the basis of previous experience,[11,15] and inspired by strategies for functional-group protection,[16] in this work, instead of using toxic and expensive organometallic compounds, we designed a facile and versatile protocol based on protected metal–organic precursors for the preparation of amino-functionalized magnetic NPs (Fe_3O_4, Mn_3O_4, and $MnFe_2O_4$) followed by removal of the protecting groups. The size, morphology, crystallite, surface chemistry, and magnetic properties of the MNPs were systematically investigated. Two representative products, Fe_3O_4 and Mn_3O_4, were used for conjugation with the target folic acid ligand (FA), and then they were utilized as targeting contrast agents for MRI of cancer cells in vitro.

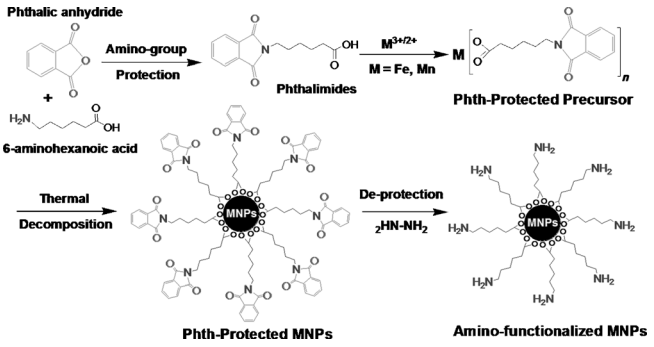

Scheme 1. Synthetic route to amino-functionalized MNPs based on a protected metal–organic precursor.

mide. Finally, the amino-functionalized MNPs can be obtained by decomposition of the Phth-protected precursor in a solvent mixture (diphenyl ether/oleylamine) followed by deprotection.

Figure 1 A and B show the FTIR spectra of the Phth-protected Fe and Mn precursors, respectively. The sharp bands centered at 1710–1720 cm^{-1} and 1770 cm^{-1} are characteristic for vibrations of metal–carboxylate bonds. The decomposition temperature of the metal–organic precursor is the key to temperature control of the reaction to form MNPs. Therefore, the thermal decomposition behavior of the solid-state metal phthalimide precursors was investigated by thermogravimetric/differential thermal analysis (TG/DTA; Figure 1 C and D), which revealed that the phthalimide ligand dissociated from the Fe precursor at 210–260 °C and from the Mn precursor around 160 °C. The Fe_3O_4 and $MnFe_2O_4$ NPs were obtained at 260 °C and the Mn_3O_4 NPs at 160 °C in diphenyl ether/oleylamine.

Results and Discussion

Synthesis of amino-functionalized MNPs

The synthetic route to amino-functionalized MNPs (MNPs-NH_2) is shown in Scheme 1. 6-Aminohexanoic acid (AHA) was chosen as the ligand for the metal because of its good water solubility and the strong coordination of its carboxyl group with metal ions, which results in orientation of the amino group to the outside of the coordination compound. However, the amino group of AHA must first be protected by changing it to phthalimide (Phth) by dehydrative condensation of AHA with phthalic anhydride. Then, the Phth-protected metal–organic precursor can be prepared by coordination of metal chloride with phthali-

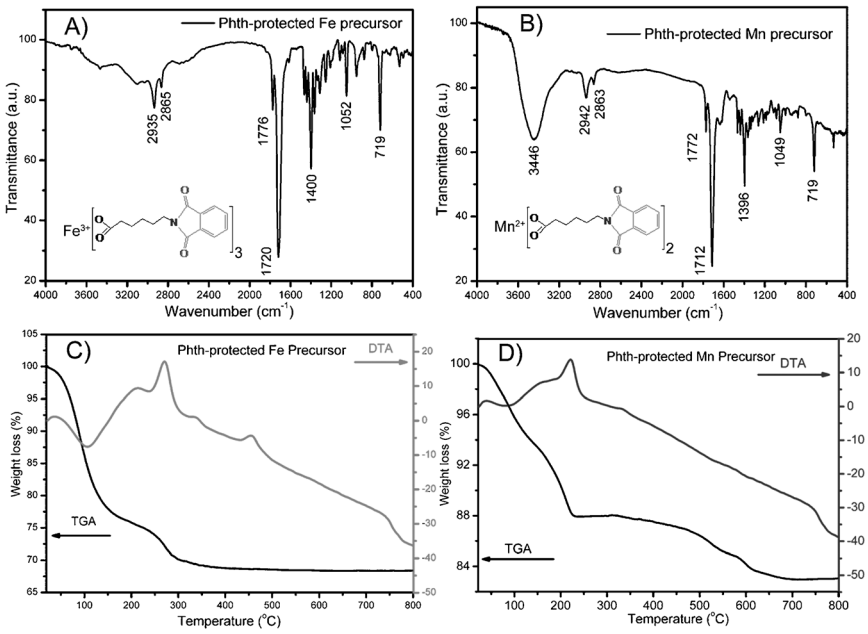

Figure 1. FTIR spectra of Phth-protected Fe (A) and Mn (B) precursors. TGA/DTA curves of Phth-protected Fe (C) and Mn (C) precursors.

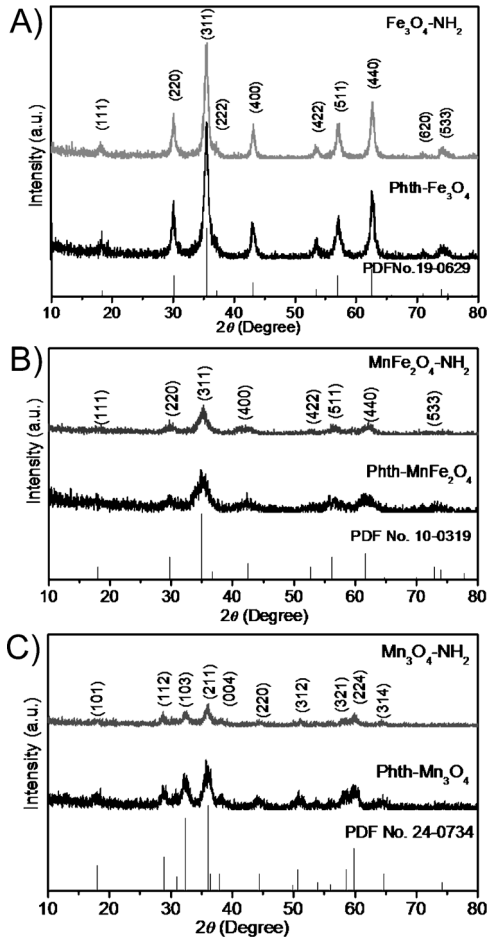

Figure 2. Powder XRD patterns of Phth-protected and amino-functionalized Fe_3O_4 (A), $MnFe_2O_4$ (B), and Mn_3O_4 (C) MNPs.

The crystallinity and structure of the Phth-protected hydrophobic and amino-functionalized hydrophilic MNPs were examined by powder XRD. The peak position and relative intensity of all diffraction peaks for Fe_3O_4 (Figure 2A), $MnFe_2O_4$ (Figure 2B), and Mn_3O_4 (Figure 2C) match well with standard powder diffraction data from JCPDS No. 19-0629, 10-0319, and 24-0734, respectively. Importantly, the XRD patterns before and after deprotection of the MNPs showed no difference. The broadening of the diffraction peaks distinctly reveals the nanocrystalline nature of the samples. Notably, the XRD pattern of Fe_3O_4 had relatively narrow peak widths and strong intensities, that is, it had high crystallinity and larger particle size. The average crystallite size calculated from the diffraction peak by using the Schërrer equation was about 13.7 nm. The slightly broader peaks of Mn_3O_4 and $MnFe_2O_4$ indicate smaller crystal sizes, which were calculated to be 5.8 and 7.1 nm, respectively.

The morphology of the as-prepared MNPs were characterized by TEM (Figure 3). The average particle sizes of the Phth-protected hydrophobic MNPs were about 14.3 nm for Fe_3O_4 (Figure 3A1), about 7.5 nm for $MnFe_2O_4$ (Figure 3B1), and about 6.6 nm for Mn_3O_4 (Figure 3C1), and they exhibited narrow size distributions and good dispersibility. After deprotection of the Phth-protected MNPs in hydrazine hydrate solution, amino-functionalized Fe_3O_4 (Figure 3A2), $MnFe_2O_4$ (Figure 3B2), and Mn_3O_4 (Figure 3C2) MNPs were obtained. The hydrophilic MNPs showed slight aggregation due to hydrogen-bonding interactions of the amino groups on the surface of the particles, but the samples still consisted primarily of single MNPs, which maintained the same particle sizes and morphologies as the hydrophobic MNPs (Supporting Information, Figure S1). Furthermore, the nanometer-scale details of the crystal-lattice fringes in the higher-magnification images of each sample confirmed the single-nanocrystal nature of the MNPs. The interplanar spacings of about 0.25 nm, about 0.298 nm, and about 0.49 nm correspond to the *d* spacings of the [311], [202], and [101] planes of Fe_3O_4, $MnFe_2O_4$, and Mn_3O_4, respectively. The hydrophobic Fe_3O_4, $MnFe_2O_4$, and Mn_3O_4 MNPs have good solubility in nonpolar solvents (e.g., $CHCl_3$), and the corresponding amino-functional MNPs were well dispersed in polar solvents (e.g., water), as can clearly be seen in Figure 3 A3, B3, and C3, respectively.

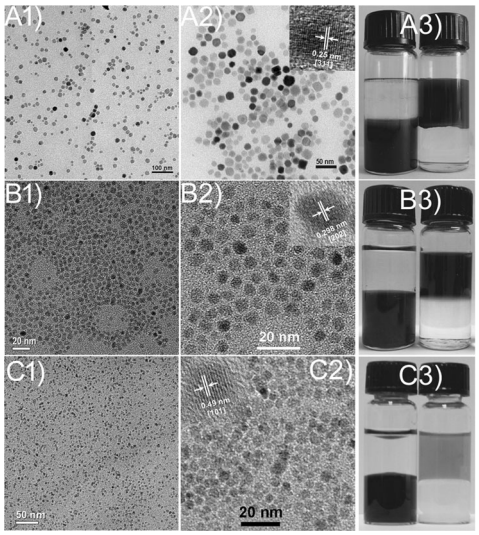

Figure 3. TEM images of Phth-protected hydrophobic Fe_3O_4 (A1), $MnFe_2O_4$ (B1), and Mn_3O_4 (C1) MNPs. The corresponding amino-functionalized hydrophilic MNPs are shown in A2), B2), and C2), respectively. The photographs in A3), B3), and C3) show the hydrophobic Fe_3O_4, $MnFe_2O_4$ and Mn_3O_4 MNPs in $CHCl_3$ (bottom layer) and the corresponding amino-functionalized MNPs in water (upper layer), respectively.

The aim of this work was to prepare amino-functionalized MNPs, and we paid more attention to the surface properties of the MNPs. To characterize the MNP surfaces, FTIR spectroscopy, which is the most direct strategy to characterize the surface chemistry of MNPs, was first utilized (Figure 4). The FTIR spectra of all samples exhibited a broad band centered at 3440 cm^{-1}, ascribed to NH_2 or OH of water. The characteristic sharp and strong peak around 1711 cm^{-1} corresponded to the phthalimide group of the Phth-MNPs. After deprotection of the Phth-MNPs in the hydrazine hydrate solution, a new band around 1579 cm^{-1} was observed, which was attributed to the vibrations of NH_2 groups on the surface of MNPs-NH_2. The absorptions at about 1436 cm^{-1} and about 854 cm^{-1} were attributed to the CH_2 groups of alkyl chains and benzene, respectively. Additionally, the surface zeta potential of each sample

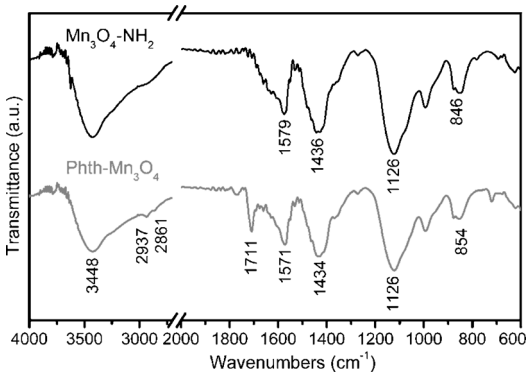

Figure 4. FTIR spectra of the Mn_3O_4 MNPs before and after deprotection.

was measured to further prove the presence of amino groups on the surfaces of the MNPs (Supporting Information, Figure S2). The surface zeta potentials of amino-functionalized Fe_3O_4, $MnFe_2O_4$, and Mn_3O_4 MNPs under neutral conditions were +14.3, +9.36, and + 15.9 mV, respectively. Finally, the amount of amino groups on the surfaces of MNPs was quantitatively determined by using the 9-fluorenylmethyl chloroformate (Fmoc-Cl) quantification protocol,[17] which gave amino-group densities of 1.2×10^{-4} mmol mg^{-1} for Fe_3O_4, 1.4×10^{-4} mmol mg^{-1} for $MnFe_2O_4$, and 1.15×10^{-4} mmol mg^{-1} for Mn_3O_4 MNPs (Supporting Information, Figure S3). On the basis of the above-described characterization, we can conclude that amino-functionalized MNPs were fabricated successfully by our newly developed protocol.

Magnetic properties of MNPs

The saturated magnetization M_s of MNPs before and after deprotection was evaluated by field-dependent magnetization measurements in the solid state at room temperature; the lack of hysteresis loops indicates the superparamagnetic nature of the Fe_3O_4 (Figure 5 A1) and $MnFe_2O_4$ (Figure 5 B1) NPs. The M_s values of Fe_3O_4 and $MnFe_2O_4$ were found to be 56.32 and 25.86 emu g^{-1} before deprotection, respectively, which are smaller than those reported in the literature.[12b,18] The lower M_s value of the MNPs is generally believed to be due to the decreased particle size and different surface properties of the particles.[18,19] However, this level of M_s is acceptable for bioapplications, in which M_s values of 7–22 emu g^{-1} are usually utilized.[20] Notably, the M_s values of Fe_3O_4 and $MnFe_2O_4$ increased to 59.76 and 28.444 emu g^{-1} after deprotection, respectively. The slight increase in M_s is attributed to hydrolysis of the protecting group, which resulted in an increased core content of the MNPs. For Mn_3O_4 NPs, the diameter of the paramagnetic threshold of the bulk particle is 7 nm.[21] The magnetic hysteresis loops of our 6.6 nm Mn_3O_4 NPs exhibited paramagnetic behavior at room temperature, as predicted (Figure 5 C1). The M_s of amino-functionalized Mn_3O_4 NPs also slightly increased compared with the Phth-protected NPs.

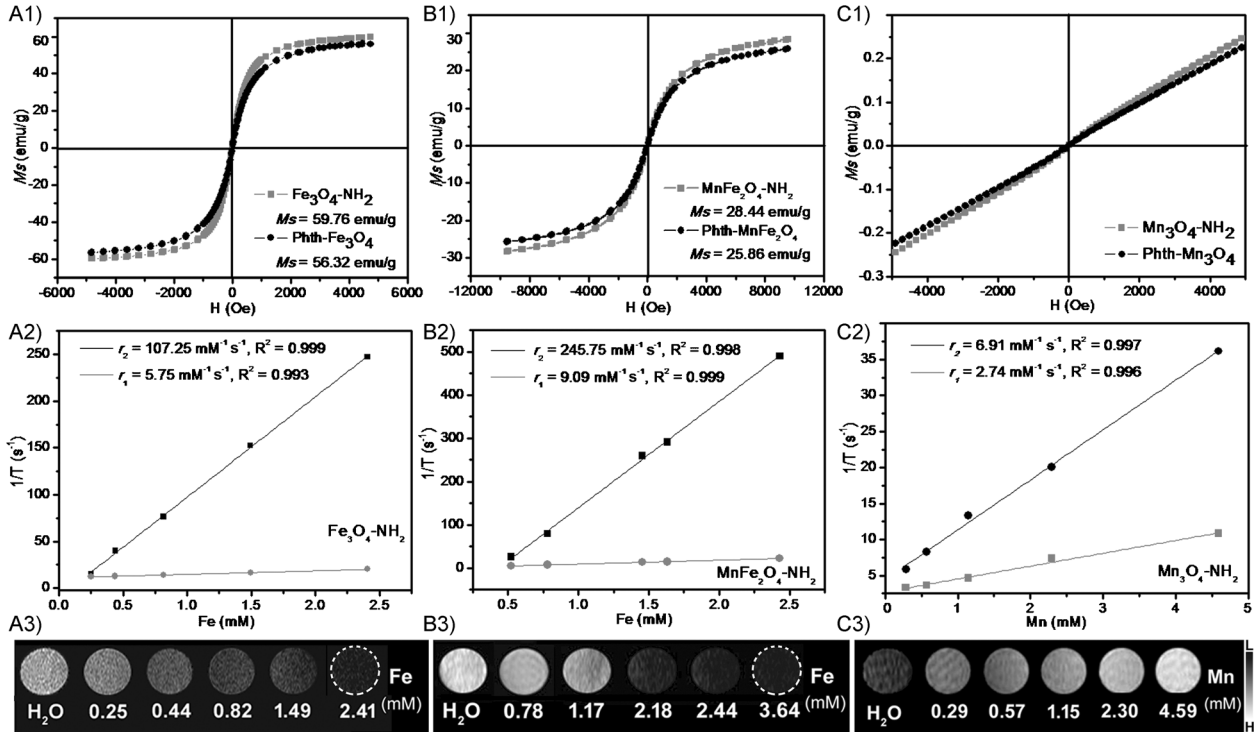

Figure 5. Magnetic properties of the MNPs. Hysteresis loops of Fe_3O_4 (A1), $MnFe_2O_4$ (B1), and Mn_3O_4 (C1) MNPs before and after deprotection at room temperature, r_1 and r_2 values of amino-functionalized Fe_3O_4 (A2), $MnFe_2O_4$ (B2), and Mn_3O_4 (C2) MNPs, T_2-weighted MRI of Fe_3O_4 (A3) and $MnFe_2O_4$ (B3), and T_1-weighted MRI of Mn_3O_4 (C3).

To evaluate the effectiveness of the MNPs as MRI agents, the relaxation properties of the amino-functionalized MNPs were examined by measuring the dependence of the longitudinal relaxation rate r_1 and transverse relaxation rate r_2 in aqueous medium at 0.5 T. The r_1 and r_2 values of Fe_3O_4 were 3.74 and 107.25 $mM^{-1}s^{-1}$ (Figure 5 A2), respectively, and those of $MnFe_2O_4$ were 7.26 and 245.75 $mM^{-1}s^{-1}$ (Figure 5 B2), respectively. The high r_2/r_1 ratios (28.7 for Fe_3O_4 and 33.8 for $MnFe_2O_4$) suggested that these NPs could be excellent negative MRI contrast agents. Figure 5 A3 and B3 show the T_2-weighted MR images of various concentrations of Fe_3O_4 and $MnFe_2O_4$ in aqueous solvents, respectively. The signal intensity was reduced and the images appeared darker as the Fe concentration increased. In contrast, by measuring the r_1 and r_2 values of Mn_3O_4 at various concentrations of Mn ions, values of $r_1 = 2.74\ mM^{-1}s^{-1}$ and $r_2 = 6.91\ mM^{-1}s^{-1}$ (Figure 5 C2) were obtained. The low r_2/r_1 ratio of 2.5 for the Mn_3O_4 MNPs indicates that they are potential positive MRI contrast agents, and they indeed resulted in signal enhancement in the T_1-weighted MR images with increasing Mn concentration (Figure 5 C3). Interestingly, the $MnFe_2O_4$ MNPs had a higher r_2 value than in our previous report,[15] and the Mn_3O_4 MNPs also had a higher r_1 value than other reported sub-10 nm materials.[17a,22] The higher r_1 and r_2 value of these MNPs can be attributed to the following two factors:[2,3b,18] 1) the high crystallinity of the MNPs, which resulted in larger magnetic motion; 2) the diffusion of water protons adjacent to the particles was accelerated due to the thin coating layer (6-aminohexanoic acid ligands) with an open molecular structure that accelerates dephasing of the proton spins and results in strong reduction of the T_2 relaxation time.[23]

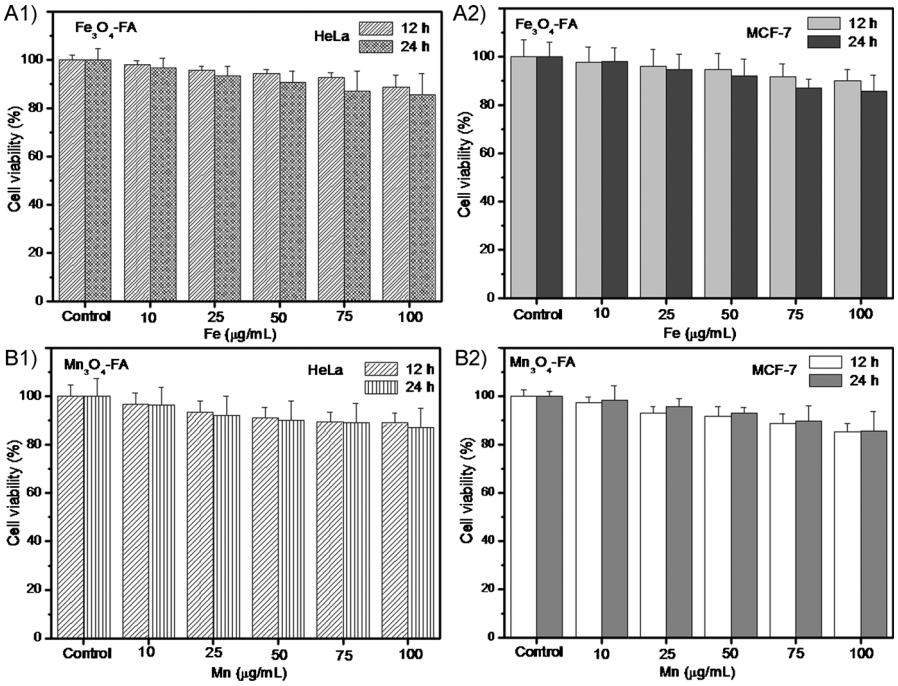

Figure 6. In vitro cell viability of HeLa and MCF-7 cells incubated with A) Fe_3O_4(RB)-FA and B) Mn_3O_4(RB)-FA at different concentrations for 12–24 h.

Biological applications

To demonstrate potential bioapplications of the amino-functionalized MNPs, they were further bioconjugated with targeting ligands and used as folic acid receptor (FAR)-targeting MRI probes in vitro. Fe_3O_4 and Mn_3O_4 NPs were chosen as T_2 and T_1 contrast agents, respectively. The two samples were first labeled with a fluorescent dye (rhodamine B: RB) as a tracer for quantitative flow-cytometric analyses of the targeting capability of the MNPs, and secondly, folic acid (FA) was labeled onto the surface of the MNPs as a targeting ligand (Figures S4–S6 of the Supporting Information). Before the FA-conjugated MNPs were used for cellular targeting MR imaging, the effect of the MNPs(RB)-FA on cell proliferation was assessed with a human cervical carcinoma cell line (HeLa) and a human breast adenocarcinoma cell line (MCF-7) by using an in vitro toxicology assay kit (TOX-1, Sigma) based on the reduction activity of methyl thiazolyltetrazolium (MTT; Figure 6). The viability of untreated cells was assumed to be 100%. On incubating the HeLa and MCF-7 cells with 100 $\mu g\,mL^{-1}$ [Fe] (or [Mn]) of the MNPs(RB)-FA, less than 10% of the cells died after 12 h of exposure, and the two cell lines also showed less than 12% loss of cell viability even after exposure for 24 h with the same concentration. These data indicate that the MNPs(RB)-FA ($\leq$100 $\mu g\,mL^{-1}$ in our experiment) have low cytotoxicity.

Then, MR imaging of both HeLa (FAR-positive) and MCF-7 (FAR-negative) cells treated with the FA-conjugated MNPs with different Fe (or Mn) concentrations (0, 10, 30, and 50 $\mu g\,mL^{-1}$) was performed by using a 0.5 T MRI system (Figure 7). The HeLa cells treated with the Fe_3O_4-FA (Figure 7 A1) and Mn_3O_4-FA (Figure 7 B1) NPs showed gradual MR signal enhancement of T_2- and T_1-weighted images, respectively, with increasing particle concentration. The signal enhancement was much greater than that of MCF-7 cells treated with the same NPs without conjugation and with similar particle concentrations. This suggests that FA-conjugated MNPs can specifically affect the MR signal through FAR-mediated binding and uptake.[17a,24] The slightly increased MR signal for MCF-7 cells treated with the MNPs at higher concentrations (50 $\mu g\,mL^{-1}$) is attributed to diffusion-induced nonspecific cellular uptake of the particles.[24–25] These results were further confirmed by quantitative analysis of the amount of iron or manganese taken up by both

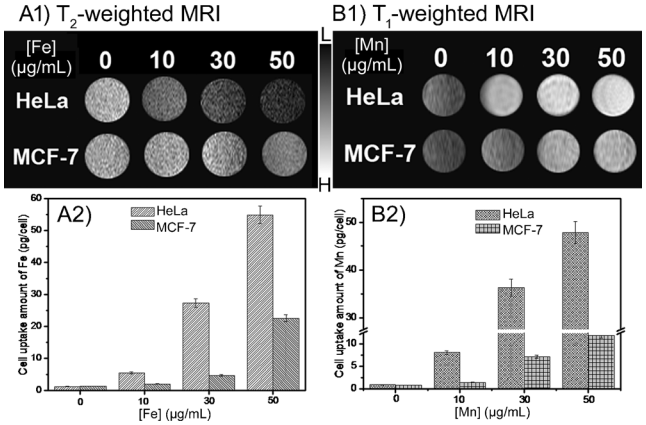

Figure 7. T_2-weighted and T_1-weighted MR images of Fe_3O_4(RB)-FA (A1) and Mn_3O_4(RB)-FA (B1) in HeLa and MCF-7 cells after incubation for 3 h (0.5 T MR system). The gray-scale bar changing from black to white indicates gradually increasing MR signal intensity. Uptake of immortalized HeLa and MCF-7 cells after incubation with different concentrations of Fe_3O_4(RB)-FA (A2) and Mn_3O_4(RB)-FA (B2).

the positive HeLa cells and the control MCF-7 cells by inductively coupled plasma atomic emission spectroscopy (ICP-AES), as shown in Figure 7 A2 and B2, respectively. At a given concentration of the FA-conjugated MNPs, the uptake of MNPs by MCF-7 cells is significantly lower than that by HeLa cells.

In addition, the targeting capability of the FA-conjugated MNPs was evaluated by flow cytometry. Figure 8 only shows the data of Fe_3O_4(RB)-FA; similar results for Mn_3O_4(RB)-FA are shown in Figure S7 of the Supporting Information. At a low dose of MNPs(RB)-FA ([Fe] (or [Mn]) = 10 μg mL^{-1}), the fluorescence intensity of the HeLa cells was about four times higher than that of the MCF-7 cells. When the Fe (or Mn) concentration of the MNPs(RB)-FA was increased to 30 μg mL^{-1}, the HeLa cells (FAR-positive) showed remarkably higher fluorescence signals than the MCF-7 cells (60.44 versus 8.81% for Fe_3O_4(RB)-FA, 66.42 versus 7.20% for Mn_3O_4(RB)-FA). On further increasing the Fe (or Mn) concentration of the particles to 50 μg mL^{-1}, the number of positively labeled HeLa cells increased to 87.36 and 94.93% for Fe_3O_4(RB)-FA and Mn_3O_4(RB)-FA, respectively, whereas the corresponding negative MCF-7 cells still remained at a low level. These results suggest that the MNPs(RB)-FA preferentially bind to HeLa cells with high-level FAR expression.[17a,24] In contrast, MCF-7 cells without FAR expression do not show significant binding to the MNPs(RB)-FA. At an Fe (or Mn) concentration of 50 μg mL^{-1}, the increased uptake (14.49% for Fe_3O_4(RB)-FA and 12.47% for Mn_3O_4(RB)-FA) in the MCF7 cells (FAR-negative cells) likely results from a concentration-induced diffusion process.[24–25] Therefore, lower concentrations of the NPs provided better targeting specificity. To optimize the particle concentration to avoid false positives for in vivo applications, we usually select the minimum concentration of the particles that can achieve saturated binding with targeted cells through flow-cytometric analysis.[17a] To further confirm whether the binding of MNPs(RB)-FA to cancer cells is receptor-mediated, free FA (2.5 mM) was preincubated with HeLa cells before incubation with MNPs(RB)-FA, so that it could block the binding sites of FARs and thereby limit the binding with the MNPs(RB)-FA. Only very weak signals of about 11.24 and 8.7% for Fe_3O_4(RB)-FA and Mn_3O_4(RB)-FA were observed, respectively, at the maximum concentration. This result further indicated that the binding of MNPs(RB)-FA was mainly mediated by receptor-mediated endocytosis.[24] The slightly nonspecific binding of MNPs(RB)-FA to HeLa cells could be due to passive uptake of nanoparticle by the cells. These quantitative analysis results further confirmed that MNPs(RB)-FA could be specially taken up by tumor cells that overexpress FAR. Therefore, all of these in vitro results clearly demonstrated that the as-prepared amino-functionalized MNPs could be further bioconjugated and used as potent targeting MRI probes.

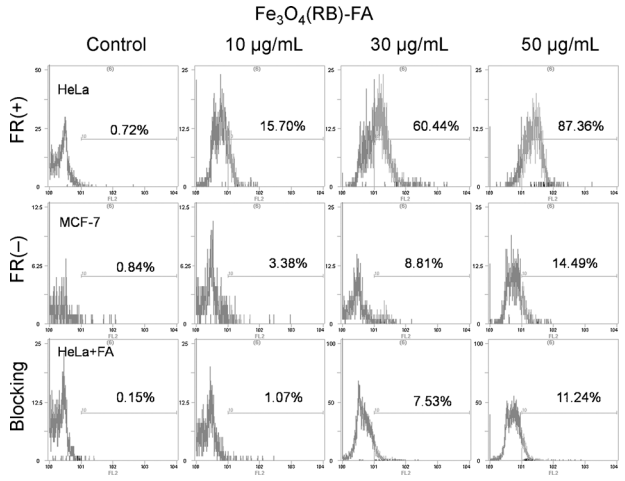

Figure 8. Flow-cytometric profiles of the cellular uptake of Fe_3O_4(RB)-FA in HeLa (FAR-positive) and MCF-7 (FAR-negative) cells with different concentrations (0, 10, 30, 50 μg mL^{-1}) in PBS at 37 °C for 3 h (*x* axis: logarithm of the fluorescence intensity; *y* axis: cell number). Blocking group: HeLa cells were preincubated with a PBS solution (2% DMSO) of FA (2.5 mM) for 1 h at 37 °C and then incubated with MNPs(RB)-FA.

Conclusion

We have presented a novel synthetic protocol for preparing water-soluble and functional Fe_3O_4, $MnFe_2O_4$, and Mn_3O_4 MNPs with particle sizes of about 14.3, 7.5, and 6.6 nm, respectively, by thermal decomposition of a phthalimide-protected precursor followed by deprotection. The amino groups on the surface of the final 6-aminohexanoic acid-coated MNPs made them water-soluble. The thin coating layer and small particle size of the prepared MNPs also resulted in a dramatic increase in the relaxivity of the $MnFe_2O_4$ (r_2 = 245.75 mM^{-1} s^{-1}) and Mn_3O_4 (r_1 = 2.74 mM^{-1} s^{-1}) MNPs. The reported methodology provides a simple, versatile, and cost-effective route for the direct synthesis of high-quality water-soluble and amino-functional MNPs, which is very important for applications of MNPs in biomedical fields. Finally, our studies have also demonstrated that the amino-functionalized MNPs could be easily bioconjugated with targeting ligands and successfully used for targeted cellular imaging, and this confirms the potential of the functional MNPs synthesized by our novel protocol in targeted imaging and therapy applications.

Experimental Section

Materials

Iron(III) trichloride, manganese(II) chloride tetrahydrate, ethanol, hexane, diphenyl ether, and folic acid (FA) were purchased from Sinopharm Chemical Reagent (Shanghai, China). 6-Aminohexanoic acid (AHA), oleylamine, and 9-fluorenylmethyl chloroformate (Fmoc-Cl) were purchased from J&K Chemical (Shanghai, China). Rhodamine B isothiocyanate (RBITC), *N*-hydroxysulfosuccinimide (Sulfo-NHS), 1-ethyl-3-(3-dimethylaminopropyl) carbodiimide hydrochloride (EDC), and hydrazine hydrate solution (78–82%) were purchased from Sigma-Aldrich (Shanghai, China). All reagents were used without further purification. Water used in all experiments was purified by using a Milli-Q Plus 185 water purification system (Millipore, Bedford, MA) to give a resistivity higher than 18 MΩ cm.

Synthesis of the Phth-protected metal–organic precursor

Firstly, the Phth-protected ligand was synthesized by dehydrative condensation of 6-aminohexanoic acid with phthalic anhydride (92.4% yield). A mixture of 6-aminohexanoic acid and phthalic anhydride in 1:1 molar ratio was heated at 170 °C for 4 h. After the mixture was cooled to room temperature, a white powder was filtered from the reaction medium, washed with deionized water, and dried in vacuum. Then, the Phth-protected metal–organic precursor was prepared by the reaction of metal ions with the Phth-protected ligand. Briefly, 3 mmol of $MnCl_2{\cdot}4H_2O$ with 6 mmol of Phth-protected ligand or 3 mmol of $FeCl_3{\cdot}6H_2O$ with 9 mmol of Phth-protected ligand were dissolved in 25 mL of CH_2Cl_2, 2.5 mL of triethylamine was added dropwise, and the reaction mixture was stirred for 5 h. The final product was washed three times with deionized water to remove residual metal ions, the solvent was removed on a rotary evaporator, and the dark brown precursor were obtained (ca. 96% yield).

Synthesis of amino-functionalized MNPs

The Phth-protected metal–organic precursor (12 mmol) was dissolved in in 20 mL of diphenyl ether/oleylamine in a 100 mL three-neck flask. The Mn_3O_4 NPs were synthesized by two-stage heating: first, the mixture was rapidly heated to 120 °C and held at that temperature for 1 h to remove the water from the solution; second, the reaction temperature was increased to 160 °C at a heating rate of 5 °C min^{-1} and maintained at that temperature for 4.5 h under a flow of nitrogen. The $MnFe_2O_4$ and Fe_3O_4 NPs were synthesized by three-stage heating: first, the reaction solution was rapidly heated to 120 °C and held at that temperature for 1 h to remove the water; second, the mixture was heated to 210 °C at a heating rate of 5 °C min^{-1} and maintained at that temperature for 2 h; third, the reaction temperature was further increased to 260 °C and kept at that temperature for 1.5 h. Diphenyl ether/oleylamine volume ratios of 20/0, 18/2, and 15/ 5 were used for the synthesis of Mn_3O_4, $MnFe_2O_4$, and Fe_3O_4 MNPs, respectively. The final reaction solution was cooled to room temperature, and the black-brown MNPs were isolated by adding an excess of ethanol followed by centrifugation and washing with ethanol and hexane three times (yield: 57–66% based on metal). The Phth-protected hydrophobic MNPs (Phth-MNPs) can be easily dispersed in nonpolar organic solvents such as hexane, toluene, and dichloromethane. The amino-functionalized MNPs were obtained by deprotection of the Phth-MNPs with hydrazine. Phth-MNPs were dispersed in 15 mL of CH_2Cl_2, a mixture of 15 mL of H_2O, 15 mL of EtOH, and 15 mL of hydrazine hydrate solution (82%) was added, and the reaction mixture vigorously stirred for 4 h. The reaction mixture was allowed to stand until completely stratified, whereby the brown amino-functionalized MNPs were transferred into the upper aqueous layer. The hydrophilic MNPs were separated and then isolated by centrifugation and washing with water and ethanol (yield: 74–77%). The obtained products were dispersed in H_2O. The amount of amino groups on the surface of MNPs was determined by using the standard Fmoc quantification protocol.[17]

Synthesis of rhodamine B and FA conjugates of Fe_3O_4 and Mn_3O_4

To modify the MNPs-NH_2 with a fluorescent dye, MNPs-NH_2 (3.6×10^{-3} mmol NH_2, ca. 30 mg Fe_3O_4 or 32 mg Mn_3O_4) was dissolved in 100 mL of dried THF, and RBITC (1.0 mg, molar ratio of RBITC/NH_2 = 1/2) was added to the solution. The mixture were stirred under nitrogen atmosphere in the dark at room temperature for 5 h. The resulting MNP(RB)-NH_2 was precipitated by centrifugation at 12000 rpm for 10 min and purified by several cycles of redispersion in ethanol and centrifugation. Then, FA was further conjugated with the remaining amino-groups of MNP(RB)-NH_2. Briefly, FA (8.0 mg, 1.8×10^{-2} mmol, molar ratio of FA/NH_2 = 10/1) was dissolved in 20 mL of anhydrous DMSO, EDC and Sulfo-NHS (molar ratio FA/EDC/Sulfo-NHS = 1/2/2.5) were added, and the mixture was stirred gently at room temperature for 3 h. 30 mg of MNP(RB)-NH_2 dissolved in 10 mL of DMSO was added to the activated FA solution, and the mixture stirred gently for another 3 h at room temperature. The final MNP(RB)-FA was separated by centrifugation at 12000 rpm for 10 min and washed three times with phosphate-buffered saline (PBS, pH 7.4). The product was dispersed in PBS and stored at 4 °C.

Cell culture

A human cervical carcinoma cell line (HeLa) and a human breast adenocarcinoma cell line (MCF-7) were provided by Shanghai Institutes for Biological Sciences (SIBS), Chinese Academy of Sciences (CAS, China). Cells were cultured in Dulbecco's modified Eagle's medium (DMEM) supplemented with 10% fetal bovine serum (FBS) at 37 °C and 5% CO_2. Cells were plated in tissue culture flasks under 100% humidity.

In vitro cytotoxicity assay

In vitro cytotoxicity of Fe_3O_4(RB)-FA and Mn_3O_4(RB)-FA was evaluated by MTT assay of HeLa and MCF-7 cells. Cells were seeded into a 96-well cell culture plates at 5×10^4 cells per well in DMEM with 10% FBS at 37 °C and 5% CO_2 for 24 h; then the cells were incubated with Fe_3O_4(RB)-FA (or Mn_3O_4(RB)-FA) with different Fe (or Mn) concentrations (0, 10, 25, 50, 75, 100 μg mL^{-1} diluted in DMEM) for 12 h or 24 h at 37 °C under 5% CO_2, respectively. Thereafter, MTT (10 mL, 5 mg mL^{-1}) was added to each well, and the plate was incubated for 4 h at 37 °C. After addition of 10% sodium dodecyl sulfate (SDS, 100 μL/well), the OD570 value (Abs.) of each well with background subtraction at 690 nm was measured on Thermo Multiskan MK3-based microplate reader. The following formula was used to calculate the inhibition of cell growth: cell viability [%] = (mean of Abs. value of treatment group/mean Abs. value of control) × 100.

In vitro MRI

HeLa and MCF-7 cells (5×10^6) were separately incubated with Fe_3O_4(RB)-FA (or Mn_3O_4(RB)-FA) with different Fe (or Mn) concentra-

tions (0, 10, 30, 50 μg mL^{-1}, diluted in PBS) for 3 h at 37 °C in cell culture medium. The cells were washed with PBS three times, and then the cells (1×10^6 cells mL^{-1}) were suspended in PBS for MR imaging. T_2- or T_1-weighted MR images were acquired by using a conventional spin–echo sequence with the following parameters: TR/TE = 500/12 ms, 220×320 matrices, 82×120 mm field of view, 140 Hz/Px of bandwidth, and slice thickness of 3 mm in a 0.5 T system (Shanghai Niumag Corporation ration NM120-Analyst).

Flow cytometry

The cell treatment was as the same as the in vitro MRI experiment, except that the block group was preincubated with a PBS solution (2% DMSO) of FA for 3 h at 37 °C. After being washed twice with PBS, the cells were suspended in PBS buffer and analyzed with a flow cytometer (Beckman Coulter, Quanta SC, USA).

Characterization

The size and morphology of prepared MNPs were observed under a JEOL JEM-2100 low- to high-resolution transmission electron microscope. XRD measurements were performed on a Bruker D4 diffractometer at a scanning rate of 1° min^{-1} in the 2θ range from 10 to 80° with graphite-monochromatized $Cu_{K\alpha}$ radiation (λ = 1.5406 nm). FTIR spectra were recorded on a Nicolet Avatar 370 with KBr pellets. TGA/DTA curves were recorded on a DTG-60H (Shimadzu) under atmospheric condition at a heating rate of 10 °C min^{-1}. The surface zeta potential was measured by using a Malvern Zetasizer Nano ZS model ZEN3600 (Worcestershire, UK) equipped with a standard 633 nm laser. The magnetic hysteresis loops were measured with a Quantum Design SQUID MPMS XL-7 magnetometer. The T_1 and T_2 relaxation times were measured on an NMR Analyzing & Imaging system NMI20-Analyst (Shanghai Niumag Corporation, 0.5 T magnet, point resolution: 156×156 μm, section thickness: 0.6 mm, TE = 60 ms, TR = 4000 ms, number of acquisitions: 1). Relaxivities r_1 and r_2 were calculated by curve fitting of $1/T_1$ and $1/T_2$ [s^{-1}] versus the Fe and Mn concentration [mM], respectively.

Acknowledgements

This work was financially supported by the National Natural Science Foundation of China (51102171, 21271130), Program for Changjiang Scholars and Innovative Research Team in University (No. IRT1269), the Key Subject of Education Ministry of China (210075), Shanghai Scientific Grant for Selection and Cultivation of Outstanding Young University Teachers (ssd10009), and the Program of Shanghai Normal University (DZL124).

Keywords: imaging agents · magnetic properties · magnetic resonance imaging · nanoparticles · protecting groups

[1] a) M. Colombo, S. Carregal-Romero, M. F. Casula, L. Gutierrez, M. P. Morales, I. B. Bohm, J. T. Heverhagen, D. Prosperi, W. J. Parak, *Chem. Soc. Rev.* **2012**, *41*, 4306–4334; b) N. A. Frey, S. Peng, K. Cheng, S. Sun, *Chem. Soc. Rev.* **2009**, *38*, 2532–2542; c) D. Ho, X. Sun, S. Sun, *Acc. Chem. Res.* **2011**, *44*, 875–882.

[2] Y.-W. Jun, J.-W. Seo, J. Cheon, *Acc. Chem. Res.* **2008**, *41*, 179–189.

[3] a) E. Terreno, D. D. Castelli, A. Viale, S. Aime, *Chem. Rev.* **2010**, *110*, 3019–3042; b) J. Kim, Y. Piao, T. Hyeon, *Chem. Soc. Rev.* **2009**, *38*, 372–390.

[4] W. B. Cai, X. Y. Chen, *Small* **2007**, *3*, 1840–1854.

[5] F. M. Kievit, M. Zhang, *Acc. Chem. Res.* **2011**, *44*, 853–862.

[6] R. Hao, R. Xing, Z. Xu, Y. Hou, S. Gao, S. Sun, *Adv. Mater.* **2010**, *22*, 2729–2742.

[7] S. Laurent, D. Forge, M. Port, A. Roch, C. Robic, L. Vander Elst, R. N. Muller, *Chem. Rev.* **2008**, *108*, 2064–2110.

[8] L. Zhou, C. Gao, X. Hu, W. Xu, *Chem. Mater.* **2011**, *23*, 1461–1470.

[9] a) H. Deng, X. Li, Q. Peng, X. Wang, J. Chen, Y. Li, *Angew. Chem.* **2005**, *117*, 2842–2845; *Angew. Chem. Int. Ed.* **2005**, *44*, 2782–2785; b) J. Liu, Z. Sun, Y. Deng, Y. Zou, C. Li, X. Guo, L. Xiong, Y. Gao, F. Li, D. Zhao, *Angew. Chem.* **2009**, *121*, 5989–5993; *Angew. Chem. Int. Ed.* **2009**, *48*, 5875–5879.

[10] T.-J. Yoon, H. Lee, H. Shao, R. Weissleder, *Angew. Chem.* **2011**, *123*, 4759–4762; *Angew. Chem. Int. Ed.* **2011**, *50*, 4663–4666.

[11] J. Park, K. An, Y. Hwang, J.-G. Park, H.-J. Noh, J.-Y. Kim, J.-H. Park, N.-M. Hwang, T. Hyeon, *Nat. Mater.* **2004**, *3*, 891–895.

[12] a) S. Sun, H. Zeng, *J. Am. Chem. Soc.* **2002**, *124*, 8204–8205; b) S. Sun, H. Zeng, D. B. Robinson, S. Raoux, P. M. Rice, S. X. Wang, G. Li, *J. Am. Chem. Soc.* **2003**, *125*, 273–279.

[13] a) Y. w. Jun, J. s. Choi, J. Cheon, *Angew. Chem. Int. Ed. Angew. Chem. In. Ed.* **2006**, *45*, 3414–3439; b) J. Park, J. Joo, S. Kwon, Y. Jang, T. Hyeon, *Angew. Chem. Int. Ed.* **2007**, *46*, 4630–4660.

[14] Z. Li, H. Chen, H. Bao, M. Gao, *Chem. Mater.* **2004**, *16*, 1391–1393.

[15] H. Yang, C. Zhang, X. Shi, H. Hu, X. Du, Y. Fang, Y. Ma, H. Wu, S. Yang, *Biomaterials* **2010**, *31*, 3667–3673.

[16] P. Y. Reddy, S. Kondo, T. Toru, Y. Ueno, *J. Org. Chem.* **1997**, *62*, 2652–2654.

[17] a) H. Yang, Y. Zhuang, H. Hu, X. Du, C. Zhang, X. Shi, H. Wu, S. Yang, *Adv. Funct. Mater.* **2010**, *20*, 1733–1741; b) H. Hu, H. Zhou, J. Liang, L. An, A. Dai, X. Li, H. Yang, S. Yang, H. Wu, *J. Colloid Interface Sci.* **2011**, *358*, 392–398.

[18] H. Hu, Z.-q. Tian, J. Liang, H. Yang, A.-t. Dai, L. An, H.-x. Wu, S.-p. Yang, *Nanotechnology* **2011**, *22*, 085707.

[19] a) U. I. Tromsdorf, N. C. Bigall, M. G. Kaul, O. T. Bruns, M. S. Nikolic, B. Mollwitz, R. A. Sperling, R. Reimer, H. Hohenberg, W. J. Parak, S. Förster, U. Beisiegel, G. Adam, H. Weller, *Nano Lett.* **2007**, *7*, 2422–2427; b) A. G. Roca, J. F. Marco, M. d. P. Morales, C. J. Serna, *J. Phys. Chem. C* **2007**, *111*, 18577–18584.

[20] L. Wang, K. G. Neoh, E. T. Kang, B. Shuter, S.-C. Wang, *Adv. Funct. Mater.* **2009**, *19*, 2615–2622.

[21] K. Dwight, N. Menyuk, *Phys. Rev.* **1960**, *119*, 1470–1479.

[22] a) H. B. Na, J. H. Lee, K. An, Y. I. Park, M. Park, I. S. Lee, D.-H. Nam, S. T. Kim, S.-H. Kim, S.-W. Kim, K.-H. Lim, K.-S. Kim, S.-O. Kim, T. Hyeon, *Angew. Chem.* **2007**, *119*, 5493–5497; *Angew. Chem. Int. Ed.* **2007**, *46*, 5397–5401; b) J. Shin, R. M. Anisur, M. K. Ko, G. H. Im, J. H. Lee, I. S. Lee, *Angew. Chem.* **2009**, *121*, 327–330; *Angew. Chem. Int. Ed.* **2009**, *48*, 321–324; c) C.-C. Huang, N.-H. Khu, C.-S. Yeh, *Biomaterials* **2010**, *31*, 4073–4078.

[23] C. Rümenapp, B. Gleich, A. Haase, *Pharm. Res.* **2012**, *29*, 1165–1179.

[24] H. Hu, L. Xiong, J. Zhou, F. Li, T. Cao, C. Huang, *Chem. Eur. J.* **2009**, *15*, 3577–3584.

[25] H. Hu, J. Sun, G. Huang, X. Li, A. Dai, H. Yang, S. Yang, *J. Mater. Sci.* **2013**, *48*, 7686–7695.

Received: December 30, 2013
Published online on April 25, 2014